Impact Response of Reinforced Concrete Beam and Its Analytical Evaluation

Kazunori Fujikake[1]; Bing Li[2]; and Sam Soeun[3]

[1]Professor, Dept. of Civil and Environmental Engineering, National Defense Academy, Yokosuka 239-8686, Japan.
[2]Associate Professor, School of Civil and Environmental Engineering, Nanyang Technological Univ., Singapore 639798, Singapore.
[3]Graduate Student, Dept. of Civil and Environmental Engineering, National Defense Academy, Yokosuka 239-8686, Japan.

Abstract

This paper examines the impact responses of reinforced concrete (RC) beams through an experimental study and presents an analytical model developed to predict the maximum midspan deflection and maximum impact load, which aids as an important performance index to evaluate the damage levels of RC beams when subjected to impact loadings. The experimental study involves a drop hammer impact test and investigates the influence of drop height and the effect of the amount of longitudinal steel reinforcement contributes to the response of RC beams. The RC beam specimens used in the experiment comprised of under-reinforced sections provided with sufficient amount of transverse reinforcements to allow for an overall flexural failure. The experimental impact responses of the RC beams were simulated with two-degree-of-freedom mass-spring-damper system model, in which the loading rate effects were duly considered. The analytical results are in good agreement with the experimental results for the RC beams that exhibited overall flexural failure.

CE Database subject headings: Concrete beams; Reinforced concrete; Impact loads; Loading rates; Deflection; Degrees of freedom.

Introduction

Some reinforced concrete (RC) structures must be designed for impact loads, which may result from the crashing of comparatively rigid heavy objects at low velocities, such as falling rocks in mountain areas and falling heavy loads dealt with in factories and warehouses due to accidents. A rational examination of the structural safety of the RC structures subjected to impact loadings is essential to develop a performance-based impact resistant design approach, in addition to currently available design specifications for impact loadings [e.g., American Association of State Highway and Transportation Officials (AASHTO) 1991; UK Atomic Energy Authority (UKAEA) 1990]. Impact loading, in general, is an extremely severe loading condition characterized by its application of a force of great intensity within a short duration. The behavior of a structural component under impact loading may consist of two response phases, as shown

in Fig. 1: the local response due to the stress wave that occurs at the loading point during a very short period after impact; and the overall response including the free vibration effect due to the elastic-plastic deformation that occurs over a long period in the whole structural member after impact. The overall response depends predominantly on the loading rate effect and the dynamic behavior of the structural component.

Overall failure tends to be a major issue concerning RC beams subjected to impact loading (e.g., Hughes and Beeby 1982; Ishikawa et al. 2000; Kishi et al. 2001; Yamamoto et al. 2003; Kishi et al. 2003). In contrast, local failure, such as penetration, scabbing, perforation and/or punching shear, tends to be the predominant mode of failure for RC plates subjected to impact loadings (e.g., Miyamoto et al. 1991; Agardh and Laine 1999; Dancygier 2000; Li and Chen 2003; Zhang et al. 2005; Dancygier et al. 2007).

A clear correlation has been established between the maximum deformation response and the degree of flexural damage to the RC beam subjected to impact loads based on previous research works (Fujikake et al. 2006). The damage levels of the RC beam vary from no damage to moderate damage, severe damage and complete collapse with increasing maximum deformation. Therefore, to properly investigate the structural safety of RC beams under impact loading, it is important to estimate both its flexural capacity and its maximum deformation response as an important damage index.

In this study, a drop hammer impact test was performed on twelve specimens of RC beams. The influence of drop height and the amount of longitudinal reinforcement on the impact responses of the RC beams was investigated. Nonlinear analysis was carried out to evaluate the flexural capacity of the RC beams with their respective loading rate effects and is subsequently presented. Finally, an analytical model to determine the maximum midspan deflection of RC beams subjected to impact loadings at its mid-span was developed.

Experimental Program

Test Specimens

The RC beam specimens as illustrated in Fig. 2 have cross-sectional dimensions of 250 mm in depth, 150 mm in width, and 1,700 mm in length. The details of the test RC beams are given in Table 1. The three variations of longitudinal reinforcement provided within the beam specimens include D13, D16, and D22 deformed bars. The yield strengths of D13, D16, and D22 were 397 MPa, 426 MPa, and 418 MPa, respectively. D10 bars spaced 75 mm apart with a yield strength of 295 MPa were used as stirrups. The bending and shear resistances for each RC beam were calculated based on JSCE Concrete Standard [Japan Society of Civil Engineers (JSCE) 2002], and tabulated in Table 2. The shear resistance varied from 50–155% larger than its bending resistance. Therefore, all RC beams are expected to be weaker in flexure (i.e., flexure controlled beams).

The mix proportion of the ready-mixed concrete used to cast the RC beams is tabulated in Table 3. The aggregates used had a maximum size of 10 mm. All tests were performed

within a period of 4 days after 70 days of casting. The concrete compressive strength at the time of testing was 42.0 MPa.

Impact Loading Test

For impact loading, a drop hammer impact loading machine was used, as shown in Fig. 3. A drop hammer with a mass of 400 kg was dropped freely onto the top surface of the RC beam at mid-span from four different heights: 0.15, 0.3, 0.6, and 1.2 m for Series S1616 beam specimens; 0.3, 0.6, 1.2, and 2.4 m for Series SI322 and Series S2222 beam specimens. The striking head of the drop hammer had a hemispherical tip with a radius of 90 mm. The RC beam was supported over a span of 1,400 mm with specially designed devices, allowing it to freely rotate while preventing it from moving out of displacement.

The contact force developed between the hammer and the RC beam was measured using a dynamic load cell, which was rigidly connected to the drop hammer. The midspan deflection response of the RC beam was measured using a laser displacement sensor. The sensor uses a thin rubber sheet mounted on the bottom of the RC beam as a target to measure the response. The computer-based data acquisition system recorded the data at a sampling rate of 100 kHz.

Experimental Results

Failure Mode

Typical failure modes obtained in the impact loading test are shown in Fig. 4. Series S1616 beams exhibited an overall flexural failure at all the drop heights. For Series SI322 and Series S2222 beams, the overall flexural failure was observed only at a drop height of no more than 0.6 m (1.97 ft). Local failure with heavily crushed concrete near the loading point was observed at a drop height of not less than 1.2 m. The longitudinal tension reinforcement ratios are 1.26% for Series S1616 beams and 2.46% for Series SI322 and Series S2222 beams. The balanced reinforcement ratio is calculated to be 4.28%. Thus, it is noteworthy that for the RC beam with an under-reinforced section (Pillai et al. 1999), increasing the amount of tensile reinforcement can cause local failure near the impact loading point. Furthermore, it is noted that the amount of longitudinal compressive reinforcement tends to affect the degree of the local failure since the length of the local failure for Series S1322 beams is approximately 20% larger than that for Series S2222 beams.

Impact Responses

Figs. 5–7 show the measured impact loads and midspan deflections in Series S1616, Series SI322, and Series S2222 beams. The measured impact loads are characterized by an initial pulselike waveform with comparatively high amplitude followed by a blunt waveform with comparatively low amplitude, as shown in many previous researches (e.g., Hughes and Beeby 1982; Ishikawa et al. 2000; Kishi et al. 2001; Yamamoto et al. 2003;

Kishi et al. 2003). The peak of the initial pulselike waveform increases with an increase in drop height, while the duration of the initial pulselike waveform is approximately 2.0 ms regardless of the drop height. The duration of the blunt waveform increases with increasing drop height, while the peaks of the blunt waveforms were approximately identified regardless of the drop heights. There is approximately a 1.0 ms time lag between the initial rises of the impact load and the midspan deflection. The maximum midspan deflection increases with an increase in drop height.

Fig. 8 shows the maximum impact load, the impulse, and the duration of the impact load, the maximum midspan deflection, and the time taken for the maximum midspan deflection obtained at each drop height. The impulse and the duration of impact load were defined, as shown in Fig. 9. At the same drop height, it is observed that the duration of impact load, the maximum midspan deflection, and the time taken for the maximum midspan deflection of Series SI616 beams are approximately 40% larger than those of Series SI322 and Series S2222 beams. The maximum impact load and the impulse at the same drop height, however, are approximately identical despite of the differences between specimens. Since the flexural rigidities (EI) of the cracked section for Series S1616, Series SI322, and Series S2222 beams are evaluated to be 4.0×10^3, 6.1×10^3, and 6.8×10^3 ($kN \cdot m^2$), respectively, the *EI* affect the duration of impact load, the maximum midspan deflection, and the time taken for the maximum midspan deflection.

Nonlinear Analysis for Flexural Capacity of Reinforced Concrete Beam under Rapid Flexural Loading

Basic assumptions

This section describes the development of a nonlinear analysis to determine the load-midspan deflection relationship of a RC beam subjected to impact load, as shown in Fig. 10. The RC beam is simply supported across its span *L*, and loaded at midspan at a constant midspan deflection rate of $\dot{\delta}$. The proposed analysis consists of (1) the determination of the moment-curvature relationship of the RC beam section by section analysis technique, in which the strain rate effects of concrete and reinforcing steel are considered; and (2) the calculation of the load-midspan deflection relationship through the moment-curvature relationship.

In section analysis, the RC beam section is divided into a number of discrete fiber elements, as shown in Fig. 11. The following classical assumptions are made to calculate the moment-curvature relationship: (1) plane sections before bending remain plane after bending; (2) stress and strain within each discrete fiber element are constant over the element, and these values are calculated at the centroid of the fiber element; (3) additional deformation due to shearing force is ignored; (4) a perfect bond exists between concrete and reinforcing steel; (5) the stress–strain curves of concrete and reinforcing steel with strain rate effects are known; and (6) the curvature varies with the constant curvature rate $\dot{\phi}$ given as a function of the constant midspan deflection rate $\dot{\delta}$, to incorporate the rate dependences of the constituent materials.

Stress-Strain Relationship of Concrete with Strain Rate Effect

As shown in Fig. 12, the following stress–strain relationship of concrete is introduced for compression under any strain rate $\dot{\varepsilon}$:

$$\sigma = \frac{AX + (B-1)X^2}{1 + (A-2)X + BX^2} f'_{\mathrm{cd}} \tag{1}$$

where A, B=constants; X=normalized strain and f'_{cd}=dynamic compressive strength corresponding to a strain rate $\dot{\varepsilon}$. The relationship given by Eq. (1) is determined by three parameters, which are the initial elastic modulus E_{0d}, the dynamic compressive strength f'_{cd}, and the strain corresponding to the dynamic compressive strength ε'_{cd}. Those parameters are given as a function of the strain rate $\dot{\varepsilon}$ as follows (Fujikake et al. 2001):

$$E_{0d} = E_0 \left(\frac{\dot{\varepsilon}}{\dot{\varepsilon}_{\mathrm{sc}}} \right)^{0.002[\log(\dot{\varepsilon}/\dot{\varepsilon}_{\mathrm{sr}})]^{1.12}} \tag{2}$$

$$f'_{\mathrm{cd}} = f'_c \left(\frac{\dot{\varepsilon}}{\dot{\varepsilon}_s} \right)^{0.006[\log \dot{\varepsilon}/\dot{\varepsilon}_{\mathrm{sr}}]^{1.05}} \tag{3}$$

$$\varepsilon'_{\mathrm{cd}} = \varepsilon'_c \left(\frac{\dot{\varepsilon}}{\dot{\varepsilon}_{\mathrm{sc}}} \right)^{-0.036+0.01 \log(\dot{\varepsilon}/\dot{\varepsilon}_{\mathrm{sr}})} \tag{4}$$

where E_0 = initial elastic modulus for static loading (MPa); $E_0 = 3{,}320\sqrt{f'_c} + 6{,}900$ (MPa); $\dot{\varepsilon}_{sc} = 1.2 \times 10^{-5}$ (1/s); f'_c = compressive strength under static loading (MPa); ε'_c=strain corresponding to f'_c; and if $\dot{\varepsilon} < \dot{\varepsilon}_{sc}$ then $E_{0d} = E_0$, $f'_{cd} = f'_c$, and $\varepsilon'_{cd} = \varepsilon'_c$. The constants A and B and the normalized strain X are defined in Table 4 (Uebayashi et al. 2001).

It is assumed that the unloading and reloading behaviors in compression follow a straight line with a slope equal to the initial elastic modulus E_{0d}, as shown in Fig. 12. In the descending branch after the dynamic compressive strength, the point corresponding to 20% of the dynamic compressive strength is defined as an ultimate state in this study.

On the other hand, as shown in Fig. 12, the stress–strain relation of concrete in tension is given as

$$\sigma = E_{0d}\varepsilon \quad \varepsilon \geq \varepsilon_{td} \tag{5a}$$

$$\sigma = \frac{\varepsilon - \varepsilon_{tu}}{\varepsilon_{tu} - \varepsilon_{td}} f_{td} \quad \varepsilon_{td} > \varepsilon \geq \varepsilon_{tu} \tag{5b}$$

$$\sigma = 0 \quad \varepsilon < \varepsilon_{tu} \tag{5c}$$

where f_{td}=dynamic tensile strength at the strain rate $\dot{\varepsilon}$; ε_{td}=strain corresponding to the dynamic tensile strength (=f_{td}/E_{0d}); and ε_{tu} =−4.0 × 10^{-4}. The dynamic tensile strength is given as (Ross et al. 1989)

$$f_{td} = f_t \exp\left[0.00126\left(\log_{10}\frac{\dot{\varepsilon}}{\dot{\varepsilon}_{st}}\right)^{3.373}\right] \tag{6}$$

in which $\dot{\varepsilon}_{st}$=1.0 × 10^{-7}; f_t=tensile strength under static loading = $f_t = -0.23 f_c'^{2/3}$ [Japan Society of Civil Engineers (JSCE) 2002]; and if $\dot{\varepsilon} < \dot{\varepsilon}_{st}$ then $f_{td} = f_t$ .It is assumed that after cracking occurs, the unloading and reloading in tension follow the straight line with a degraded elastic modulus, as shown in Fig. 12.

Stress-Strain Relationship of Reinforcing Steel with Strain Rate Effect

For reinforcing steel, a bilinear stress–strain relationship is adopted, as shown in Fig. 13. It is assumed that the elastic modulus E_s and the strain hardening modulus E_{sp} are independent of loading rates following the experimental results by Limberger et al. (1982) and Ammann et al. (1982). The effect of the loading rate on the yield strength is considered. The following formulation proposed by Takahashi [Japan Society of Civil Engineers (JSCE) 1993] is adopted to determine dynamic yield strength (f_{syd}):

$$f_{syd} = f_{sys}(1.202 + 0.040 \times \log_{10}\dot{\varepsilon}) \geq f_{sys} \tag{7}$$

where f_{syd} = dynamic yield strength at any strain rate $\dot{\varepsilon}$ and f_{sys} = static yield strength.

Finally, the stress–strain relationship for reinforcing steel is given as

$$\sigma = E_s \times \varepsilon \quad \text{for} \quad \varepsilon \leq \varepsilon_{syd} \tag{8a}$$

$$\sigma = f_{syd} + E_{sp}(\varepsilon - \varepsilon_{syd}) \quad \text{for} \quad \varepsilon > \varepsilon_{syd} \tag{8b}$$

in which ε_{syd} = strain corresponding to the dynamic yield strength: $\varepsilon_{syd} = f_{syd}/E_s$ and E_{sp} = strain hardening modulus. It is also assumed that after yielding, the unloading and reloading follow the straight line with a slope equal to E_s.

Relationship between Midspan Deflection Rate and Curvature Rate

When section analysis is performed on a simply supported RC beam subjected to a rapid flexural load at midspan, as shown in Fig. 10, the relationship between the midspan deflection rate ($\dot{\delta}$) of the RC beam and the curvature rate ($\dot{\phi}$)at the section is required to calculate the strain rate at each fiber element in this analysis. Based on the linear elastic theory, the relationship between the midspan deflection and the curvature, as shown in Fig. 10, can be given as (Gere 2003)

$$\phi = \frac{M}{EI} = \frac{12}{L^2}\delta \tag{9}$$

In a similar manner, it is simply assumed that the following relationship exists between the curvature rate $\dot{\phi}$ and the midspan deflection rate $\dot{\delta}$

$$\dot{\phi} = \frac{12}{L^2}\dot{\delta} \tag{10}$$

This assumption seems to be reasonable because the influence of loading rate on the mechanical properties of RC is expressed as a function of the logarithmic value of the strain rate.

Analytical Moment-Curvature Relationship

Dividing the RC section into *n*-fiber concrete elements and *m*-fiber rebar elements, as shown in Fig. 11, an axial load and bending moment acting on the section at any curvature ϕ are given as

$$N = \int_A \sigma dA = \sum_{i=1}^{''} \sigma_{c.i} A_{c.i} + \sum_{j=1}^{'''} \sigma_{s.j} A_{s.j} \tag{11}$$

$$M = \int_A \sigma y dA = \sum_{i=1}^{''} \sigma_{c.i} y_{c.i} A_{c.i} + \sum_{j=1}^{'''} \sigma_{s.j} y_{s.j} A_{s.j} \tag{12}$$

where $\sigma_{c.i}$ = stress acting on the *i*th concrete fiber element; $A_{c.i}$ =area of the *i*th concrete element; $\sigma_{s.j}$ = stress of the *j*th rebar fiber element; $A_{s.j}$ = area of the jth rebar element; $y_{c.i}$ =distance from the extreme compression fiber to the centroid of the *i*th concrete fiber element; and $y_{s.j}$ =distance from the extreme compression fiber to the centroid of the *j*th rebar fiber element. In the beam member, the condition of N=0 must be satisfied by adjusting a neutral axis depth y_0 as no axial force is acted on the section.

From a linear distribution of strains across the section depth in the assumptions, the strains of the *i*th concrete fiber element and of the *j*th rebar element can be expressed as

$$\varepsilon_{c.i} = (y_0 - y_{c.i}) > \phi \tag{13a}$$

$$\varepsilon_{s.j} = (y_0 - y_{s.j}) > \phi \tag{13b}$$

where y_0= distance from the extreme compression fiber to the neutral axis and ϕ =curvature of the section.

From the basic assumptions, strain rates vary linearly with depth at the section as well. Once the curvature rate $\dot{\phi}$ is given by Eq. (10), the strain rate at each fiber element is determined as

$$\dot{\varepsilon}_{c.i} = |(y_0 - y_{c.i})| > \dot{\phi} \tag{14a}$$

$$\dot{\varepsilon}_{s.j} = |(y_0 - y_{s.j})| > \dot{\phi} \tag{14b}$$

Therefore, the stresses of any concrete fiber element and of any rebar element $(\sigma_{c.i}, \sigma_{s.j})$are calculated with the strains $(\varepsilon_{c.i}, \varepsilon_{s.j})$and the strain rates $(\dot{\varepsilon}_{c.i}, \dot{\varepsilon}_{s.j})$of the corresponding elements.

Analytical Load-Midspan Deflection Relationship

The load-midspan deflection relationship of a RC beam subjected to rapid flexural loading at the midspan deflection rate $\dot{\delta}$ is calculated based on the moment-curvature relationship obtained from the section analysis at the curvature rate $\dot{\phi}$ given by Eq. (10). The midspan deflection of the RC beam can be calculated by integrating the curvature distribution over one-half the length of the RC beam. The curvature distribution is determined from the moment distribution corresponding to the impact load applied and taking the boundary conditions into consideration. In the calculation, a constant curvature region with a length L_p is taking place at mid-span for expressing the plastic deformation within a plastic hinge region. The length of the plastic hinge region may be given as (Mattock 1967)

$$L_p = d + 0.05L \tag{15}$$

in which d = effective depth and L = span

Verification

A rapid flexural loading test on the same RC beams S1616, S1322, and S2222 used in the impact loading test were employed to validate the developed analysis approach. In the test, the RC beams were simply supported over a span of 1,400 mm (66.9 in.) and loaded

at midspan at the midspan deflection rates of 5.0×10^{-4} and 2.0 m/s (1.64×10^{-3} and 6.56 ft/s). The load acting on the RC beam was measured through a load cell. The deformation response of the RC beam was measured by using a laser displacement transducer at midspan. In the measured load, the inertia load evaluated from acceleration, which was derived as second-order derivations of the measured midspan deflection with respect to time, was eliminated from the measured load to evaluate the influence of the loading rate on the true bending resistance of the RC beam (Banthia et al. 1989).

The proposed analysis was applied to the experimental data. The calculations were carried out until the extreme compression fiber reached to the ultimate state. The elastic and strain hardening modulus of the reinforcing bars were 200 GPa and 3 GPa, respectively. The concrete compressive strength was 42 MPa. Figs. 14–16 show the experimental and the analytical results. As shown in Figs. 14–16, the influence of dynamic vibrations is still observed in the experimentally obtained load-midspan deflection relationships at the midspan deflection rate of 2.0 m/s, while the inertia loads were delaminated assuming the first mode vibration. These vibration effects may result from the higher frequency modes of more than the third vibration mode, which cannot be delaminated by the inertia correction method based on the first vibration mode. However, it can be seen that the analytical results are in good agreement with the averaged experimental results for all cases. The experimentally obtained load-midspan deflection relationships have enough load carrying capacity even after reaching a midspan deflection of 30 or 40 mm. Thus, the analytically calculated ultimate midspan deflections seem to be practical.

Analytical Evaluation of the Response of Reinforced Concrete Beam under Impact Loading

Impact Response Analysis

The RC beam subjected to the drop hammer impact at midspan may be modeled by two-degree-of-freedom mass-spring-damper system, as illustrated in Fig. 17 (Fujikake 2007). This analytical model can represent not only the overall response of the RC beam but also the local response at the contact point between the drop hammer and the RC beam with the least degrees of freedom. The spring k_1 expresses the load-midspan deflection relationship of the RC beam with loading rate effects determined from the nonlinear analysis described in the previous section. After the drop hammer with an initial impact velocity v_{ib} hits the RC beam at midspan, the RC beam, and the drop hammer move together with the same velocity v_{ia}. This assumes a perfectly plastic collision (Suzuki et al. 1996). From the conservation of momentum law, the velocity v_{ia} is given as

$$v_{\mathrm{ia}} = \frac{m_2}{m_1 + m_2} v_{\mathrm{ib}} \tag{16}$$

where m_1=equivalent mass of RC beam (=$17\rho A_c L/35$=60 kg; ρ=density of RC beam=2,400 kg/m^3, A_c=sectional area of RC beam) and m_2=mass of hammer (=400 kg). The mid-span deflection rate of the RC beam yields a maximum value just after impact

and becomes zero at the maximum midspan deflection. Thus, the midspan deflection rate of the RC beam should be changing continuously. In this study, the load-midspan deflection relationship of the RC beam is evaluated on the assumption that the RC beam deforms at the velocity v_{ia} given by Eq. (16). This assumption is reasonable because the influence of loading rate on the mechanical properties of the RC beam is expressed as a function of the logarithmic value of the strain rate. The contact spring k_2 is assumed to be 120,000 kN/m based on Hertz's contact theory (Timoshenko and Goodier 1984). The damping coefficients c_1 and c_2 are assumed to be 0 and one-half of a critical damping coefficient for the part expressing the local response given as the following equation, respectively.

$$c_2 = \sqrt{\frac{m_1 m_2}{m_1 + m_2} k_2} \tag{17}$$

The analytical impact responses in the impact load and midspan deflection and those obtained from the impact test are shown in Figs. 5–7. The analytical results were shown to be in good agreement with the experimental results when the RC beams exhibited only an overall flexural failure. There was, however, a big difference between the analytical and experimental midspan deflection responses of Series 1322 and S2222 beam specimens when subjected to a drop height of 2.4 m. It exhibited both local failure near the impact loading point and an overall flexural failure mode. The local failure observed in the RC beams was presumed to have been formed at the first peak of the impact load, which is approximately 400 kN. Therefore, as a result of a large consumption of total impact energy input used to form the local failure shortly after impact, the experimental maximum midspan deflection appeared to be small as compared to that of the analytical one. The experimental maximum midspan deflections for Series S1322 and S2222 beam specimens subjected to a drop height of 2.4 m are approximately 33% and 18% smaller than the analytical ones, respectively. The fact that the extent of the local failure for Series S1322 beam specimens was larger than that of the Series S2222 beam specimens, it is suggested that the difference in maximum midspan deflections between the experiment and the analysis is lager for Series S1322 beam specimens as compared to the Series S2222 ones.

Dissipation Energy and Analytical Model for Maximum Midspan Defelction

Typical time variations of energy calculated by a two-degree-of-freedom mass-spring-damper system model are shown in Fig. 18. At the maximum midspan deflection, the strain energy stored by spring k_1 reaches its highest value; and the kinetic energy of m_1 and m_2 comes to zero. It should be noted that the energy dissipated by dashpot c_2 reaches approximately 13% of the initial impact energy given by $m_2 v_{ib}^2$ /2. In the two-degree-of-freedom model analysis, energy obtained by summing up the energy dissipated by damper c_2 and the energy stored within spring k_2 until the maximum midspan deflection is defined as dissipation energy. Fig. 19 shows the relationship between the dissipation energy and the drop height. The dissipation energy linearly increases with an increase in drop height, as illustrated in Fig. 19.

On the other hand, assuming a perfectly plastic collision be-tween the drop hammer and the RC beam, energy loss can be calculated by

$$E_R = \frac{m_1 m_2}{2(m_1 + m_2)} v_{ib}^2 \tag{18}$$

where $v_{ib} = \sqrt{2gh}$ (g= acceleration of gravity, h= drop height).

The relationship given by Eq. (18) is shown in Fig. 19. As can be seen in Fig. 19 that the dissipation energy calculated by the two-degree-of-freedom model fits with the relationship given by Eq. (18). Therefore, the following energy conservation equation can be drawn with consideration given to dissipation energy:

$$\frac{m_2 v_{ib}^2}{2} - E_R + (m_1 + m_2) g \delta_{max} = \int_0^{\delta_{max}} P(\delta) d\delta \tag{19}$$

where g =acceleration of gravity and $P(\delta)$=load (P)-midspan deflection (δ) relationship for the spring k_1.

Eq. (19) provides a means to calculate the maximum midspan deflection of a RC beam subjected to impact loading without using the impact response analysis with the two-degree-of-freedom system model. The maximum midspan deflections estimated by the two-degree-of-freedom model analysis and Eq. (17), and those obtained from the impact test are shown in Fig. 20. The analytical results were shown to be in good agreement with the experimental results when the RC beams exhibited only an overall flexural failure.

Tables 5–7 summarizes the analytically obtained maximum midspan deflections (δ_{max}) and ultimate midspan deflections (δ_u), together with the velocities of the drop hammer just before and after impact (v_{ib}, v_{ia}). The ultimate midspan deflections for Series S1616, S1322, and S2222 beam specimens were estimated to be about 15.7 mm, 11.5 mm, and 14.1 mm, respectively. The ultimate drop height, defined as the drop height at which the maximum midspan deflection equaled to the ultimate midspan deflection, for Series S1616, S1322, and S2222 beam specimens are estimated to be 0.48 m, 0.6 m, and 0.76 m, respectively. The maximum midspan deflection exceeded the ultimate midspan deflection when the hammer was dropped at a height higher than the ultimate height.

In this proposed analytical procedure, the examination of the structural safety for the RC beam under impact loading is made possible by comparing the analytical maximum deformation response with its ultimate deformation capability, as shown in Fig. 21. For example, in Table 5, the maximum midspan deflections at a drop height not more than 0.3 m are smaller than the ultimate midspan deflections; these cases can be considered safe. The maximum midspan deflections for Series S1322 and S2222 beam specimens at a drop height of 2.4 m exceed the corresponding ultimate midspan deflections, as shown in Tables 6 and 7; these cases can be considered unsafe. It is, however, currently impossible to determine the allowable impact load shown in Fig. 21 as a criterion for the local failure. Thus, it warrants further research on the local failure.

Conclusions

Based on the results presented in this paper, the following conclusions were drawn:

1. The amount of longitudinal reinforcement significantly affected the failure modes of RC beams under impact loading. The RC beam with comparatively lower amounts of longitudinal steel reinforcement exhibited only overall flexural failure, while the RC beam with the comparatively higher amounts of longitudinal reinforcement exhibited not only the overall flexural failure but also local failure located near impact loading point due to the large impact from the loading acting on a single point.
2. The amount of longitudinal compression reinforcement affected the degree of the local failure. Local failure was substantially reduced when heavy longitudinal compression reinforcement was provided. Thus, it can be concluded that compression reinforcement helps to increase the resistance of a beam local response when subjected to impact loading.
3. The following characteristics of impact responses: the maximum impact load, the impulse, the duration of impact load, the maximum midspan deflection, and the time taken for the maximum midspan deflection increased as the drop height was increased. The duration of impact load, the maximum midspan deflection, and the time taken for the maximum midspan deflection were affected by the flexural rigidity of the RC beams.
4. A nonlinear analysis was carried out to determine the load-midspan deflection relationship of the RC beam and the effects of loading rates were developed.
5. An analytical model was developed to determine the maximum midspan deflection. The maximum midspan deflection is an important index for evaluating damage levels of RC beams subjected to impact loading. The analytical model was shown to be in good agreement with the experimental mid-span deflection when the RC beams exhibited only an overall flexural failure.
6. It was observed that the local failure was formed shortly after impact by comparing the analytical midspan deflections to those obtained from the experiments conducted.

Acknowledgements

The writers thank K. Masuda and K. Hagishima, who are former students in the National Defense Academy, Japan for their assistance in performing the impact loading test and rapid loading test.

Notation

The following symbols are used in this paper:

A = constant for stress–strain relationship of concrete;
A_c = cross section area of RC beam;
$A_{c,i}$ = area of the ith concrete fiber element;
$A_{s,j}$ = area of the jth rebar fiber element;
B = constant for stress–strain relationship of concrete;
c_1 = damping coefficient for overall response;
c_2 = damping coefficient for local response;
d = effective depth;
E_s = elastic modulus of reinforcing steel;
E_{sp} = strain hardening modulus of reinforcing steel;
E_0 = initial elastic modulus of concrete under static loading;
E_{0d} = initial elastic modulus of concrete at strain rate $\dot{\varepsilon}$;
EI = flexural rigidity;
f'_c = compressive strength of concrete under static loading;
f'_{cd} = dynamic compressive strength of concrete at strain rate $\dot{\varepsilon}$;
f_{syd} = dynamic yield strength of reinforcing steel at any strain rate $\dot{\varepsilon}$;
f_{sys} = yield strength of reinforcing steel under static loading;
f_t = tensile strength of concrete under static loading;
f_{td} = dynamic tensile strength of concrete at strain rate $\dot{\varepsilon}$;
g = acceleration of gravity;
k_1 = load-midspan deflection relationship of RC beam;
k_2 = load-displacement relationship of contact spring;
L = span;
L_p = length of plastic hinge region;
M = bending moment;
m_1 = equivalent mass of RC beam;
m_2 = mass of hammer;
N = axial load;
$P(t)$ = load eliminating inertia load;
$P_i(t)$ = inertia load;
$P_m(t)$ = load measured by a load cell;
$P(\delta)$ = load-midspan deflection relationship;
u_1 = midspan deflection of RC beam;
u_2 = displacement of drop hammer;
X = normalized strain;
v_{ia} = velocity of hammer and RC beam just after impact;
v_{ib} = velocity of drop hammer just before impact;
$y_{c,i}$ = distance from the extreme compression fiber to the centroid of the ith concrete fiber element;
$y_{s,j}$ = distance from the extreme compression fiber to the centroid of the jth rebar fiber element;
$\alpha_0(t)$ = acceleration at midspan;
δ = midspan deflection of RC beam;

δ_{max} = maximum midspan deflection of RC beam;
δ_u = ultimate midspan deflection of RC beam;
$\dot{\delta}$ = midspan deflection rate of RC beam;
ε = strain;
$\varepsilon_{c,i}$ = strain of the ith concrete fiber element;
$\varepsilon_{s,j}$ = strain of the jth rebar fiber element;
ε_{syd} = strain corresponding to dynamic yield strength of reinforcing steel;
ε_{td} = strain corresponding to dynamic tensile strength of concrete;
ε_{tu} = critical tensile strain of concrete ($=-4.0\times10^{-4}$);
ε'_c = strain corresponding to static compressive strength of concrete;
ε'_{cd} = strain corresponding to dynamic compressive strength of concrete;
$\dot{\varepsilon}$ = any strain rate;
$\dot{\varepsilon}_{c,i}$ = strain rate of the ith concrete fiber element;
$\dot{\varepsilon}_{sc}$ = reference strain rate ($=1.2\times10^{-5}/s$) for concrete in compression;
$\dot{\varepsilon}_{st}$ = reference strain rate ($=1.0\times10^{-7}/s$) for concrete in tension;
$\dot{\varepsilon}_{s,j}$ = strain rate of the jth rebar fiber element;
ρ = density of RC beam;
σ = stress;
$\sigma_{c,i}$ = stress acting on ith concrete fiber element;
$\sigma_{s,j}$ = stress of jth rebar fiber element;
ϕ = curvature; and
$\dot{\phi}$ = curvature rate.

References

[1] Agardh, L., and Laine, L. (1999). "3D FE-simulation of high-velocity fragment perforation of reinforced concrete slabs." *Int. J. Impact Eng*., 22, 911–922.

[2] American Association of State Highway and Transportation Officials (AASHTO). (1991). *Guide specifications and commentary for vessel collision design of highway bridges*, AASHTO, Washington, D.C.

[3] Ammann, W., Mühlematter, M., and Bachmann, H. (1982). "*Stress-strain behaviour of non-prestressed and prestressed reinforcing steel at high strain rates*." *Proc., RILEM/CEB/IABSE/IASS Interassociation Symp. on Concrete Structures under Impact and Impulsive Loading*, BAM, Berlin, 146–156.

[4] Banthia, N. P., Mindess, S., Bentur, A., and Pigeon, M. (1989). "Impact testing of concrete using a drop-weight impact machine." *Exp. Mech*., 29(1), 63–69.

[5] Dancygier, A. N. (2000). "Scaling of non-proportional non-deforming projectiles impacting reinforced concrete barriers." *Int. J. Impact Eng*., 24, 33–55.

[6] Dancygier, A. N., Yankelevsky, D. Z., and Jaegermann, C. (2007). "Response of high performance concrete plates to impact of non-deforming projectiles." *Int. J. Impact Eng*., 34, 1768–1779.

[7] Fujikake, K. (2007). "Response analysis of RC beams subjected to impact loads." *Proc., 1st Int. Workshop on Performance, Protection, and Strengthening of Structures under Extreme Loading* (CD-ROM), Univ. of British Columbia, Vancouver.

[8] Fujikake, K., Mori, K., Uebayashi, K., Ohno, T., and Mizuno, J. (2001). "Constitutive model for concrete materials with high-rates of loading under tri-axial compressive stress states." *Proc., 3rd Int. Conf. on Concrete under Severe Conditions*, Vol. 1, JSCE, Tokyo, 636–643.

[9] Fujikake, K., Senga, T., Ueda, N., Ohno, T., and Katagiri, M. (2006). "Study on impact responses of reactive powder concrete beam and its analytical model." *J. Adv. Concr. Technol*., 4(1), 99–108.

[10] Gere, J. M. (2003). *Mechanics of materials*, 6th Ed., Brooks/Cole, Belmont.

[11] Hughes, G., and Beeby, A. W. (1982). "Investigation of the effect of impact loading on concrete beams." *Struct. Eng*., 60B(3), 45–52.

[12] Ishikawa, N., Katsuki, S., and Takemoto, K. (2000). "Dynamic analysis of prestressed concrete beams under impact and high speed loadings." *Proc., 6th Int. Conf. on Structures under Shock and Impact*, WIT Press, Southampton, 247–256.

[13] Japan Society of Civil Engineers (JSCE). (1993). "Impact behavior and design of structures." *Structural Engineering Series 6*, JSCE, Tokyo (in Japanese).

[14] Japan Society of Civil Engineers (JSCE). (2002). *Standard specifications for concrete structures 2002, structural performance verification*, JSCE, Tokyo (in Japanese).

[15] Kishi, N., et al. (2003). "Round robin analysis of RC beam subjected to an impact load due to a falling weight." *Proc., 1st Int. Conf. on De-sign and Analysis of Protective Structure against Impact/Impulsive/ Shock Loads*, DAPSIL, Tokyo, 305–318.

[16] Kishi, N., Ikeda, K., Mikami, H., and Yamaguchi, E. (2001). "Dynamic behavior of RC beams under steel weight impact loading-effects of nose-shape of steel weight." *Proc., 3rd Int. Conf. on Concrete Under Severe Conditions,* Univ. of British Columbia, Vancouver, 660–667.

[17] Li, Q. M., and Chen, X. W. (2003). "Dimensionless formulae for penetration depth of concrete target impacted by a non-deformable projectile." *Int. J. Impact Eng*., 28, 93–116.

[18] Limberger, E., Brandes, K., and Herter, J. (1982). "Influence of mechanical properties of reinforcing steel on the ductility of reinforced concrete beams with respect to high strain rates." *Proc., RILEM/CEB/ IABSE/IASS Interassociation Symp. on Concrete Structures under Impact and Impulsive Loading*, BAM, Berlin, 134–145.

[19] Mattock, A. H. (1967). "Discussion of 'rotational capacity of reinforced concrete beams.'" *J. Struct. Div*., 93(ST2), 519–522.

[20] Miyamoto, A., King, M. W., and Fujii, M. (1991). "Analysis of failure modes for reinforced concrete slabs under impulsive loads." *ACI Struct. J*., 88(5), 538–545.

[21] Pillai, S. U., Kirk, D. W., and Erki, M. A. (1999). *Reinforced concrete design*, 3rd Ed., McGraw-Hill Ryerson, Toronto.

[22] Ross, C. A., Thompson, P. Y., and Tedesco, J. W. (1989). "Split-Hopkinson pressure-bar tests on concrete and mortar in tension and compression." *ACI Mater*. J., [23] 86(5), 475–481.

Suzuki, S., Katsuki, S., Ishikawa, N., Ishikawa, Y., and Furukawa, K. (1996). "A fundamental study on local dissipated energy and rheology model at impact point of concrete specimen by the pendulum impact test." *Journal of Structural Mechanics and Earthquake Engineering*, 36(543), 91–105 (in Japanese).

[24] Timoshenko, S. P., and Goodier, J. N. (1984). *Theory of elasticity*, 3rd Ed., McGraw-Hill Int., Singapore.

[25] Uebayashi, K., Fujikake, K., Ohno, T., Mizuno, J., and Suzuki, A. (2001). "Stress-strain model with dynamic strain softening behaviors for concrete materials under triaxial compressive stress states." *Journal of Materials, Concrete Structures and Pavements*, 50(669), 135–148 (in Japanese).

[26] U.K. Atomic Energy Authority (UKAEA). (1990). *Guidelines for the Design and Assessment of Concrete Structures Subjected to Impact*, SRD, Cheshire.

[27] Yamamoto, M., Masuya, H., and Nishimura, Y. (2003). "A study on the impact test method and characteristics of impact behavior of various reinforced concrete beams." *Proc., 1st Int. Con. on Design and Analysis of Protective Structure against Impact/Impulsive/Shock Loads*, DAPSIL, Tokyo, 245–255.

[28] Zhang, M. H., Shim, V. P. W., Lu, G., and Chew, C. W. (2005). "Resistance of high-strength concrete to projectile impact." *Int. J. Impact Eng*., 31, 825–841.

List of Tables

List of Figures

Designation	Compression side		Tension side	
	Number and size (mm)	Area A_s' (mm^2)	Number and size (mm)	Area A_s (mm^2)
S1616	2-D16	397	2-D16	397
S1322	2-D13	126.7	2-D22	774
S2222	2-D22	774	2-D22	774

Table 1

Designation	Bending resistance R_M=4 Mu/L (kN)	Shear resistance R_S=2 Vu (kN)	R_S/R_M
S1616	91.1	232.0	2.55
S1322	162.2	245.4	1.51
S2222	162.6	245.4	1.51

Table 2

W/C (%)	Unit weight (kg/m^3)					Air (%)	Slump (cm)
	W	C	S	G	Ad		
44.5	185	416	726	943	4.16	4.5	15.5

Note: W=water; C=cement; S=sand; G=gravel; and Ad=Admixture.

Table 3

Ascending portion ($\varepsilon \leq \varepsilon'_{cd}$)	Descending portion ($\varepsilon > \varepsilon'_{cd}$)
$A = E_{0d}\varepsilon'_{cd}/f'_{cd}$, $B = (A-1)^2/0.55 \geq 1-A$, $X = \varepsilon/\varepsilon'_{cd}$	$A = E_{0d}\varepsilon'_{cd}/f'_{cd}$, $B = 1$, $X = (\varepsilon/\varepsilon'_{cd})^m$ where $m = 1.04 + 2 \times (f'_{cd}/100)^2$

Table 4

Drop height (m)	v_{ib} (m/s)	v_{ia} (m/s)	δ_u (mm)	δ_{max} [a] (mm)	δ_{max} [b] (mm)
0.15	1.72	1.49	15.5	5.8	6.1
0.30	2.43	2.10	15.6	10.2	10.5
0.60	3.43	2.97	15.7	18.8	19.2
1.20	4.85	4.21	15.8	36.0	36.6

[a]By two-degree-of-freedom analysis.

[b]By Eq. (19).

Table 5

Drop height (m)	v_{ib} (m/s)	v_{ia} (m/s)	δ_u (mm)	δ_{max} [a] (mm)	δ_{max} [b] (mm)
0.30	2.43	2.10	11.2	6.3	6.7
0.60	3.43	2.97	11.4	11.3	11.7
1.20	4.85	4.21	11.6	21.3	21.8
2.40	6.86	5.95	11.8	41.2	41.7

[a]By two-degree-of-freedom analysis.

[b]By Eq. (19).

Table 6

Drop height (m)	v_{ib} (m/s)	v_{ia} (m/s)	δ_u (mm)	δ_{max} [a] (mm)	δ_{max} [b] (mm)
0.30	2.43	2.10	13.9	6.3	6.6
0.60	3.43	2.97	14.0	11.2	11.5
1.20	4.85	4.21	14.1	20.7	21.1
2.40	6.86	5.95	14.3	39.6	40.1

[a]By two-degree-of-freedom analysis.

[b]By Eq. (19).

Table 7

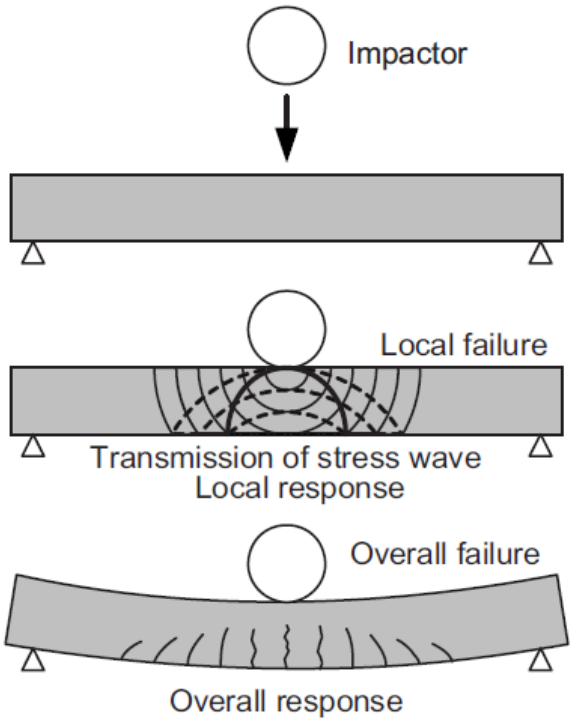
Impactor
Local failure
Transmission of stress wave
Local response
Overall failure
Overall response

Fig. 1

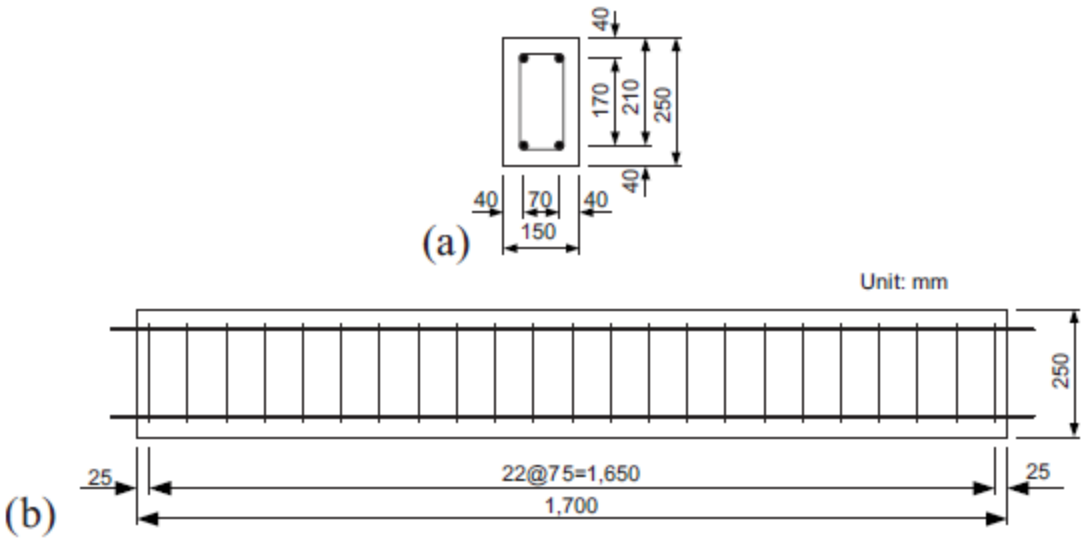

Fig. 2

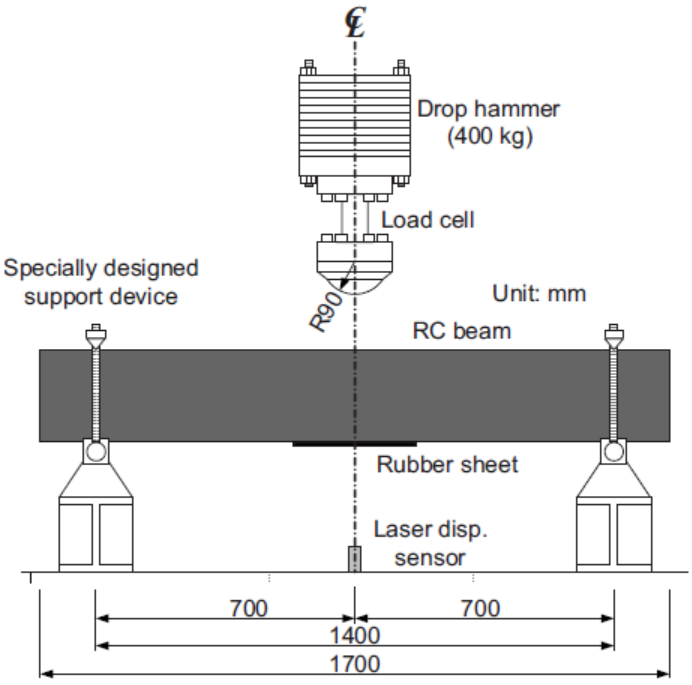
℄
Drop hammer
(400 kg)
Load cell
Specially designed
support device
R90
Unit: mm
RC beam
Rubber sheet
Laser disp.
sensor
700
700
1400
1700

Fig. 3

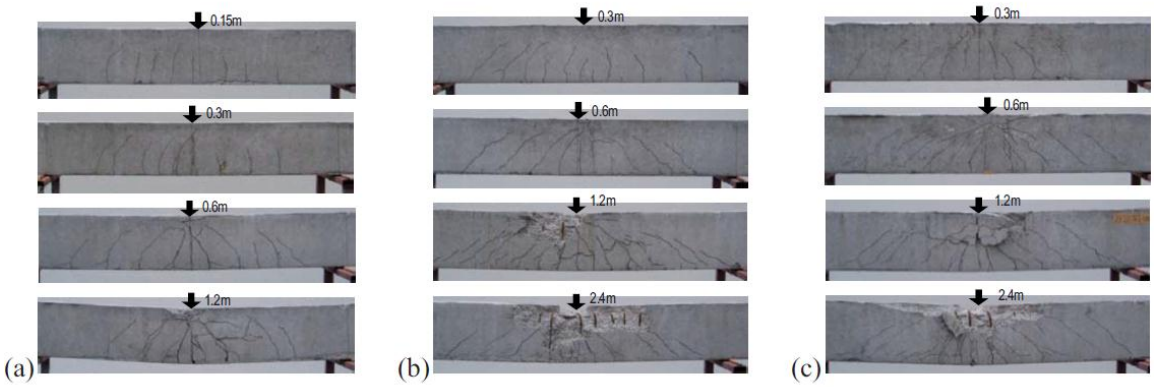

Fig. 4

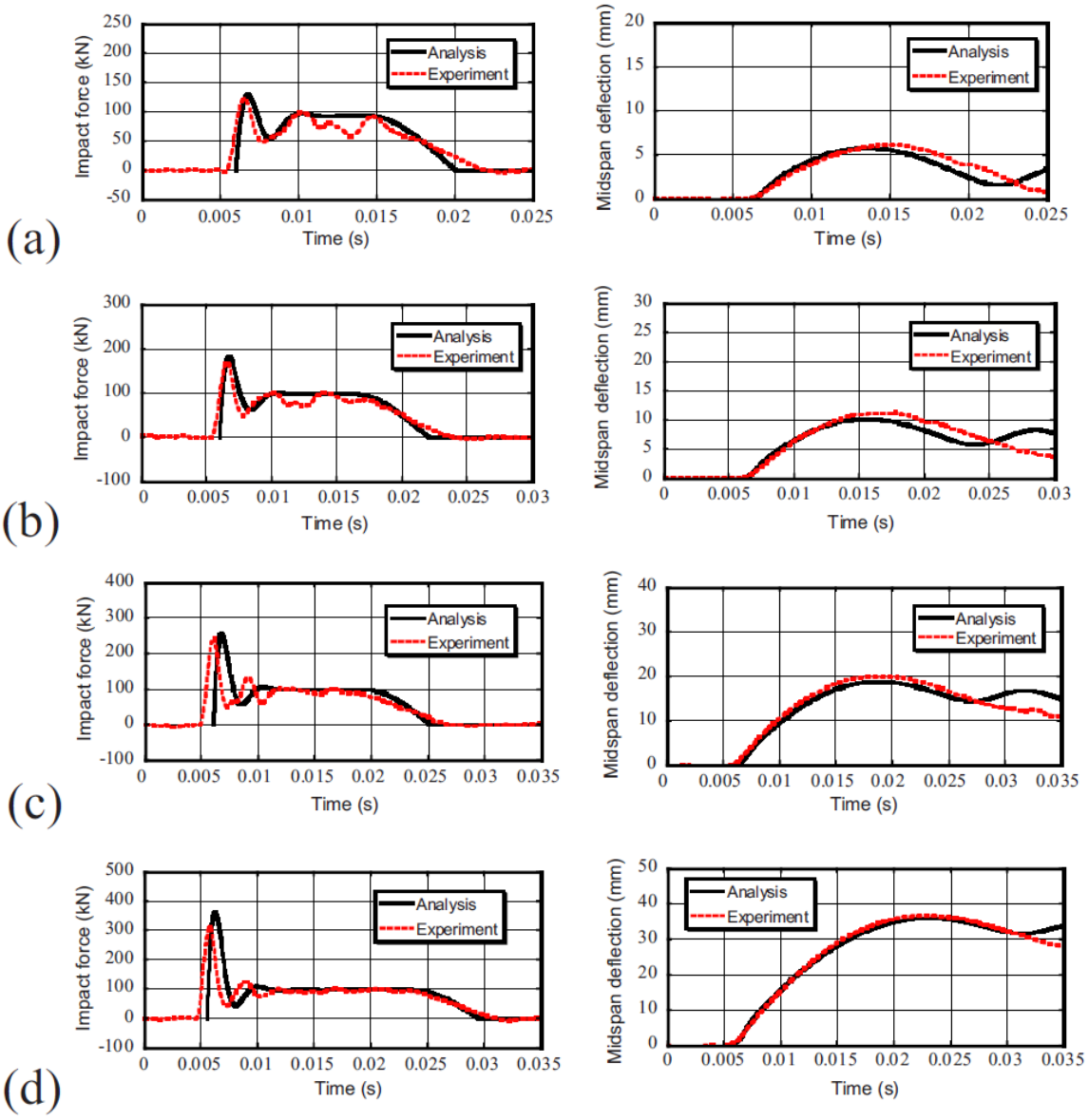
(a)
Impact force (kN)
Time (s)
Analysis
Experiment
Midspan deflection (mm)
Time (s)
Analysis
Experiment
(b)
Impact force (kN)
Time (s)
Analysis
Experiment
Midspan deflection (mm)
Time (s)
Analysis
Experiment
(c)
Impact force (kN)
Time (s)
Analysis
Experiment
Midspan deflection (mm)
Time (s)
Analysis
Experiment
(d)
Impact force (kN)
Time (s)
Analysis
Experiment
Midspan deflection (mm)
Time (s)
Analysis
Experiment

Fig. 5

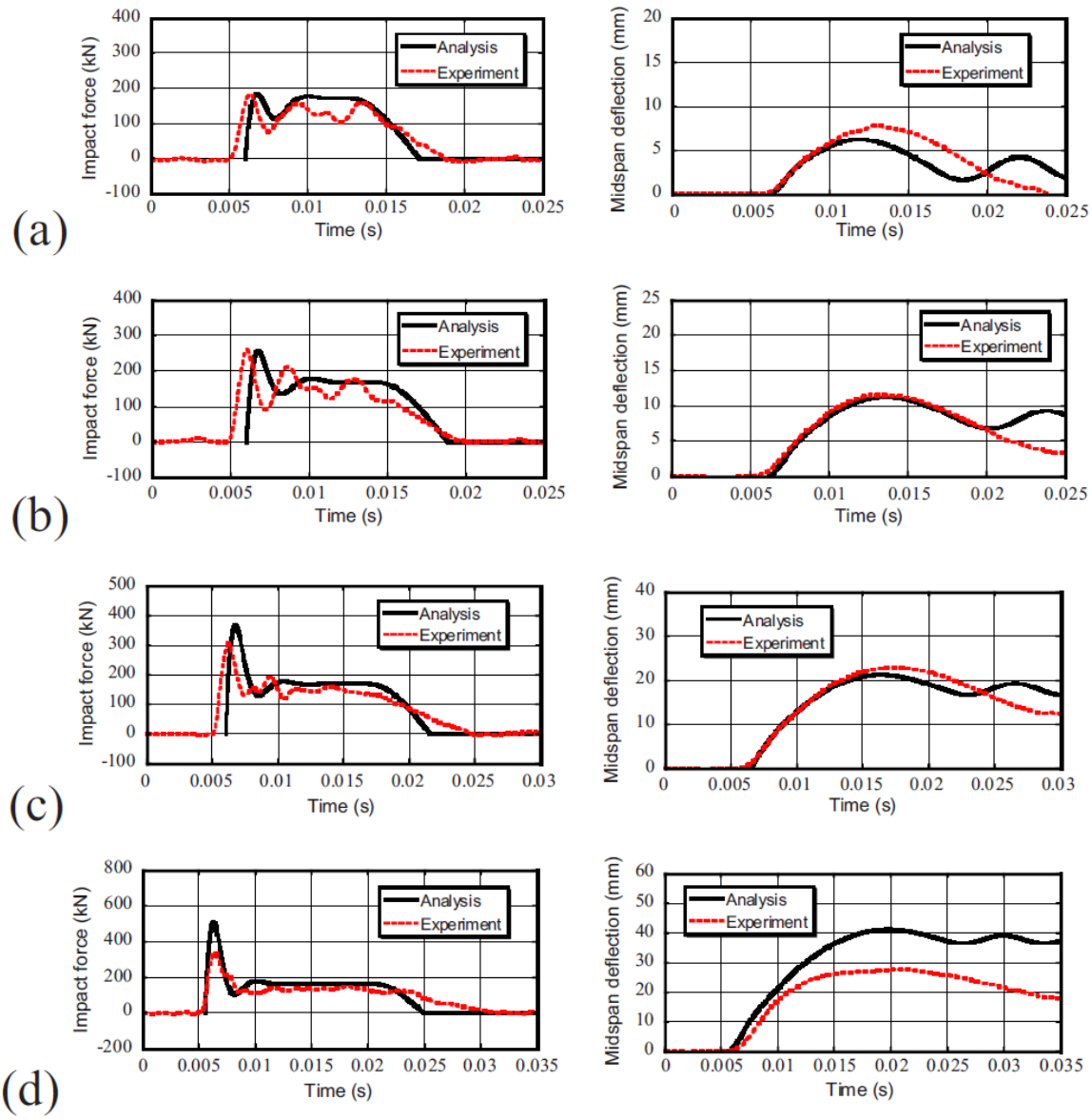
(a)
Impact force (kN)
Time (s)
Analysis
Experiment
Midspan deflection (mm)
Time (s)
Analysis
Experiment
(b)
Impact force (kN)
Time (s)
Analysis
Experiment
Midspan deflection (mm)
Time (s)
Analysis
Experiment
(c)
Impact force (kN)
Time (s)
Analysis
Experiment
Midspan deflection (mm)
Time (s)
Analysis
Experiment
(d)
Impact force (kN)
Time (s)
Analysis
Experiment
Midspan deflection (mm)
Time (s)
Analysis
Experiment

Fig. 6

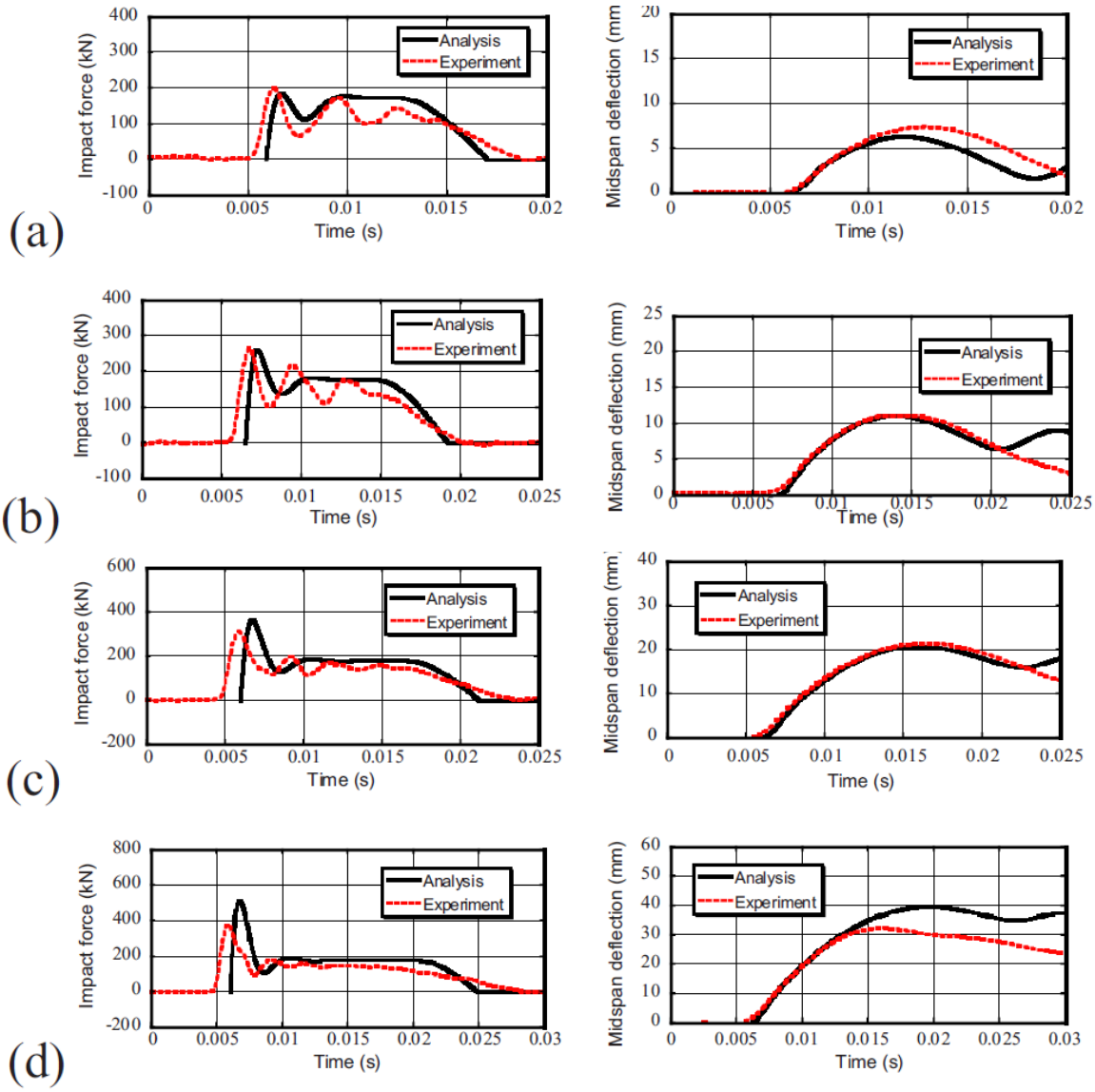
(a)
Impact force (kN)
Time (s)
Analysis
Experiment
Midspan deflection (mm
Time (s)
Analysis
Experiment
(b)
Impact force (kN)
Time (s)
Analysis
Experiment
Midspan deflection (mm)
Time (s)
Analysis
Experiment
(c)
Impact force (kN)
Time (s)
Analysis
Experiment
Midspan deflection (mm)
Time (s)
Analysis
Experiment
(d)
Impact force (kN)
Time (s)
Analysis
Experiment
Midspan deflection (mm)
Time (s)
Analysis
Experiment

Fig. 7

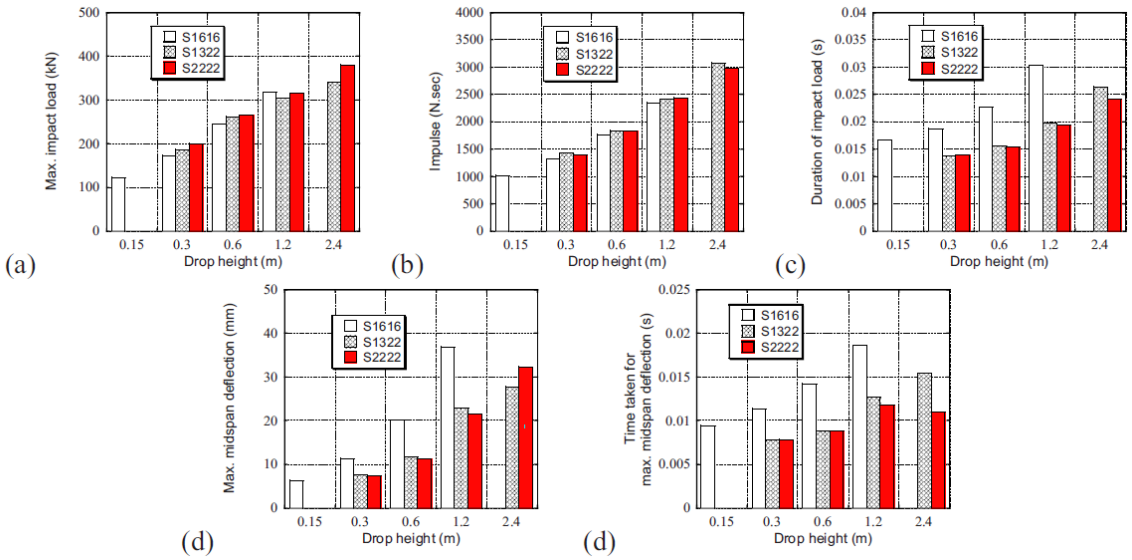
(a)
Max. impact load (kN)
S1616
S1322
S2222
Drop height (m)
(b)
Impulse (N.sec)
(c)
Duration of impact load (s)
(d)
Max. midspan deflection (mm)
(d)
Time taken for max. midspan deflection (s)

Fig. 8

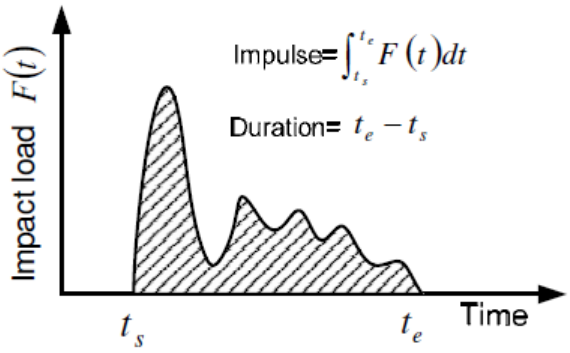
Impact load $F(t)$
Impulse= $\int_{t_s}^{t_e} F(t)dt$
Duration= $t_e - t_s$
t_s
t_e
Time

Fig. 9

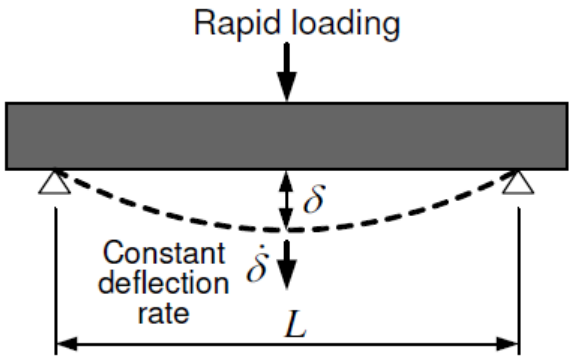

Fig. 10

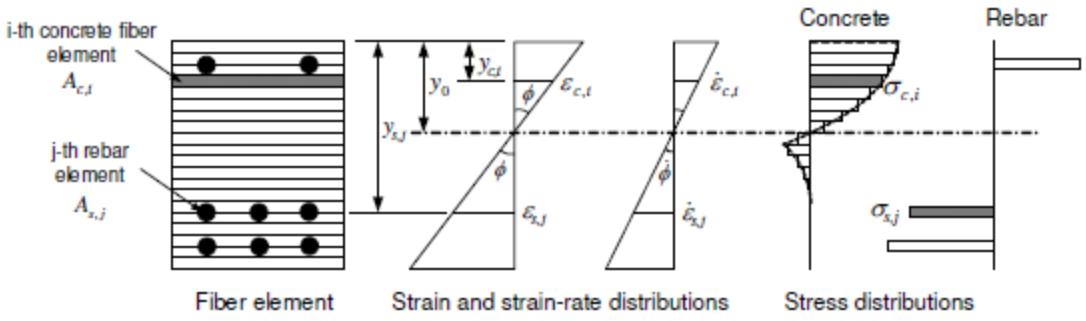
i-th concrete fiber element
$A_{c,i}$
j-th rebar element
$A_{s,j}$
$y_{c,i}$
y_0
$y_{s,j}$
ϕ
$\varepsilon_{c,i}$
$\varepsilon_{s,j}$
$\dot{\varepsilon}_{c,i}$
$\dot{\varepsilon}_{s,j}$
Concrete
Rebar
$\sigma_{c,i}$
$\sigma_{s,j}$
Fiber element
Strain and strain-rate distributions
Stress distributions

Fig. 11

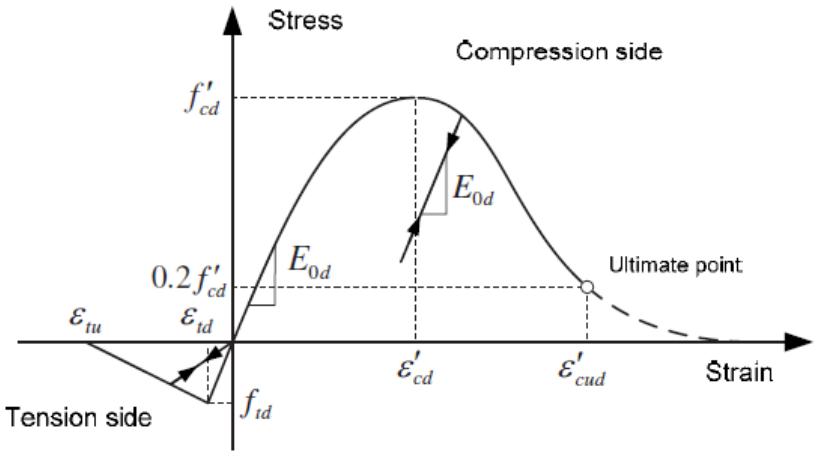
Stress
Compression side
f'_{cd}
E_{0d}
E_{0d}
$0.2f'_{cd}$
Ultimate point
ε_{tu}
ε_{td}
ε'_{cd}
ε'_{cud}
Strain
f_{td}
Tension side

Fig. 12

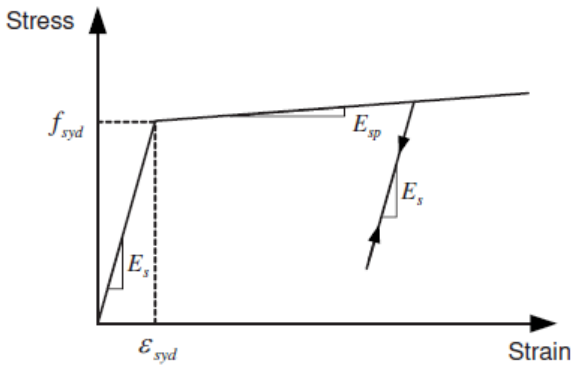

Fig. 13

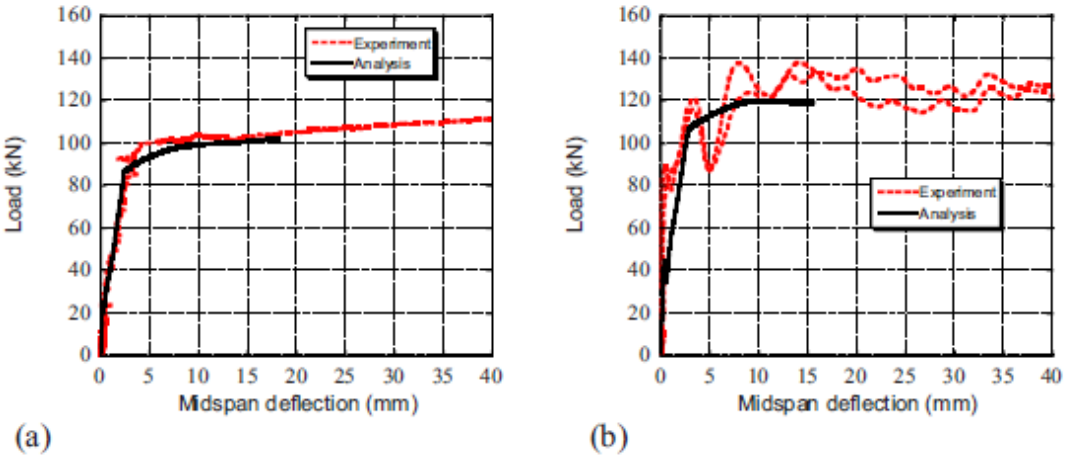

Fig. 14

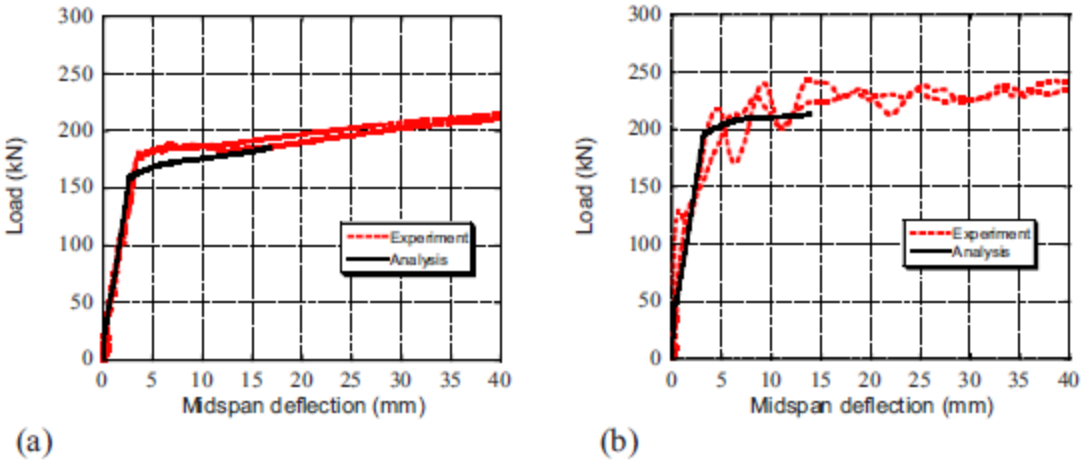

Fig. 15

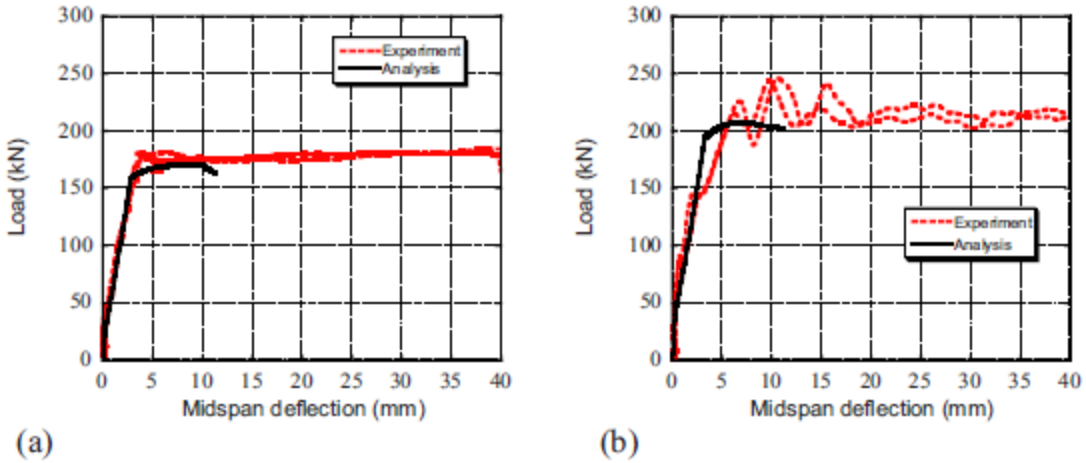

Fig. 16

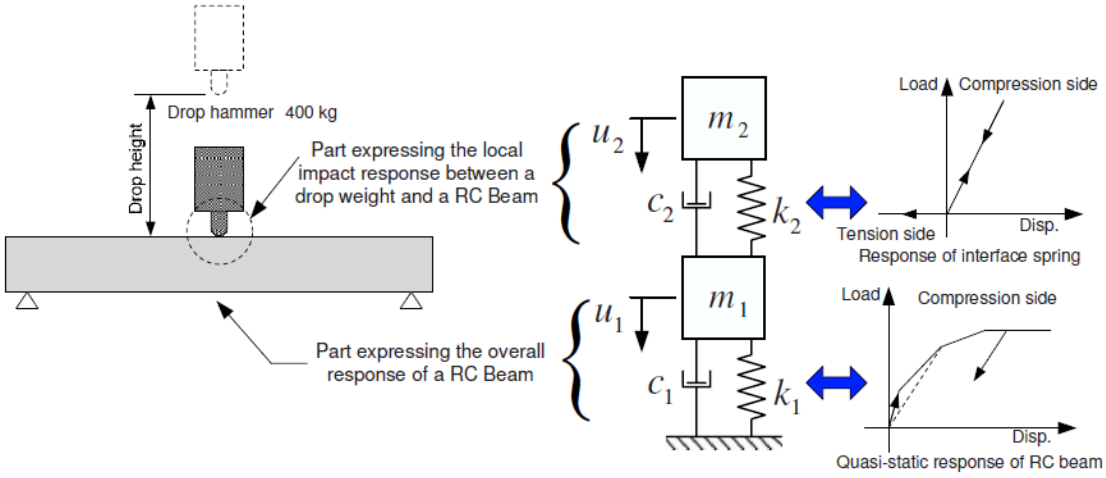
Drop hammer 400 kg
Drop height
Part expressing the local impact response between a drop weight and a RC Beam
Part expressing the overall response of a RC Beam
u_2
m_2
c_2
k_2
u_1
m_1
c_1
k_1
Load
Compression side
Tension side
Disp.
Response of interface spring
Load
Compression side
Disp.
Quasi-static response of RC beam

Fig. 17

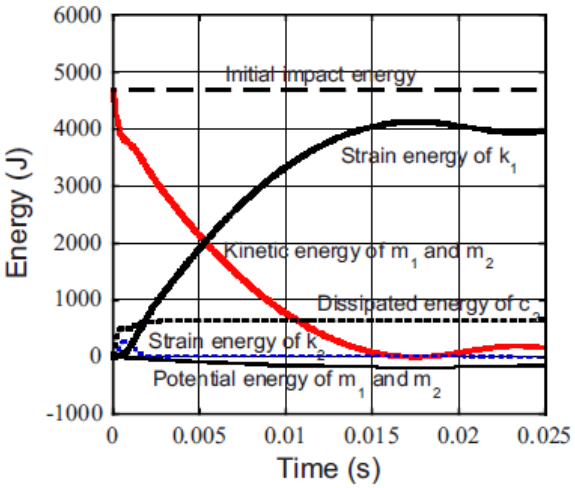
6000
5000
4000
3000
2000
1000
0
-1000
Energy (J)
0
0.005
0.01
0.015
0.02
0.025
Time (s)
Initial impact energy
Strain energy of k1
Kinetic energy of m1 and m2
Dissipated energy of c2
Strain energy of k2
Potential energy of m1 and m2

Fig. 18

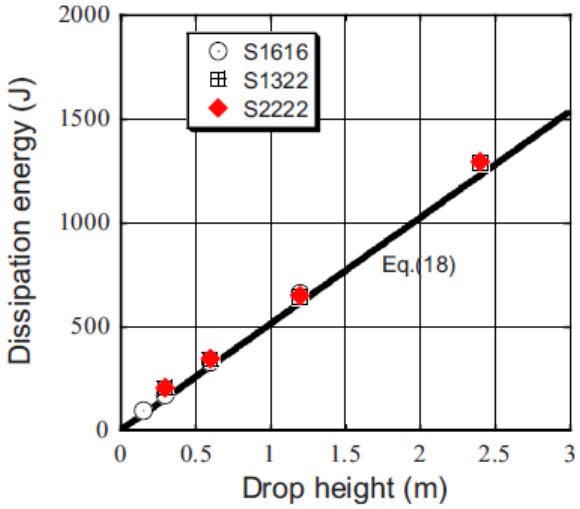
2000
1500
1000
500
0
0
0.5
1
1.5
2
2.5
3
Dissipation energy (J)
Drop height (m)
S1616
S1322
S2222
Eq.(18)

Fig. 19

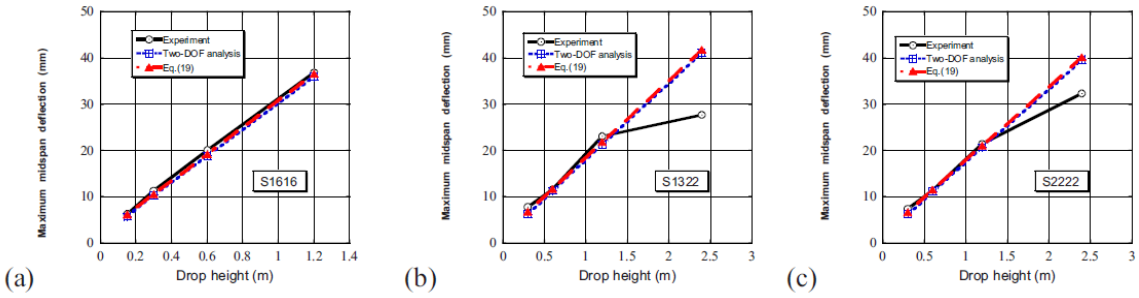
Maximum midspan deflection (mm)
Experiment
Two-DOF analysis
Eq.(19)
S1616
Drop height (m)
(a)
S1322
(b)
S2222
(c)

Fig. 20

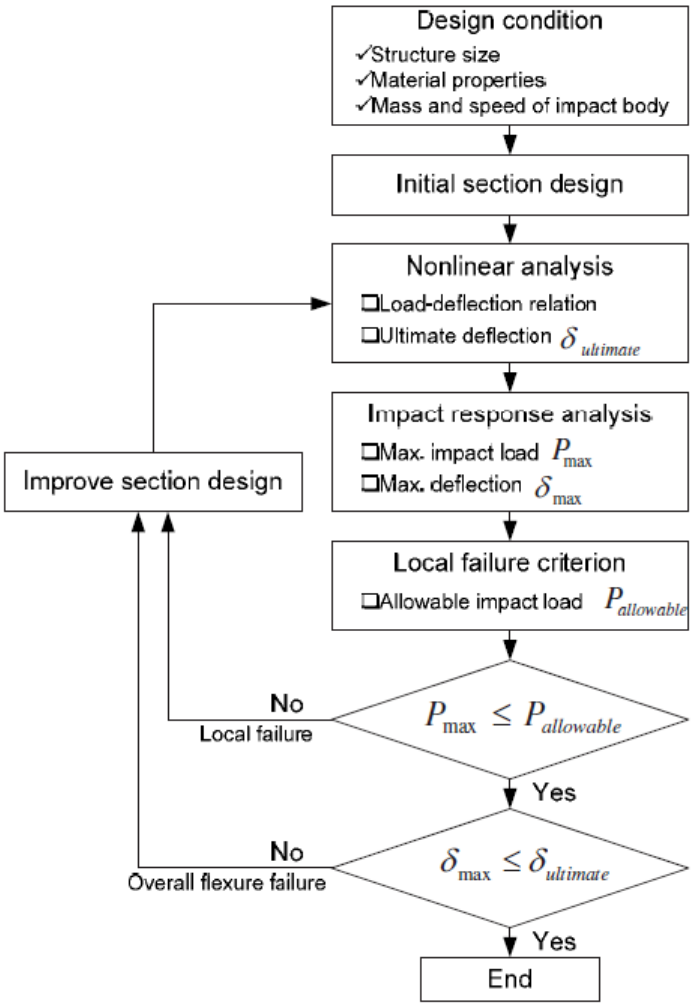
Design condition
✓Structure size
✓Material properties
✓Mass and speed of impact body
Initial section design
Nonlinear analysis
❑Load-deflection relation
❑Ultimate deflection $\delta_{ultimate}$
Impact response analysis
❑Max. impact load P_{max}
❑Max. deflection δ_{max}
Local failure criterion
❑Allowable impact load $P_{allowable}$
$P_{max} \leq P_{allowable}$
No
Local failure
Improve section design
Yes
$\delta_{max} \leq \delta_{ultimate}$
No
Overall flexure failure
Yes
End

Fig. 21